Processing–Crystallization Kinetics–Morphology Relationships in Injection Molding of PP and GFRPP

WEN-YEN CHIU,* HORNG-JER TAI, LEO-WANG CHEN, and LINE-HWA CHU

Department of Chemical Engineering, National Taiwan University, Taipei, Taiwan, Republic of China

SYNOPSIS

The dynamic crystallization model proposed in our previous work was applied to the simulation of crystallization kinetics and morphology of PP and PP/glass fiber composite (GFRPP) in injection molding process. The cooling rate was very rapid in the processing, either in the core or in the skin region of thin disc part, so that the crystallization would take place at low temperatures and the size of spherulites was small. However, the ultimate crystallinity of PP could always be obtained since the crystallization rate of PP was extremely fast. Prediction of the crystallization morphology from the dynamic model agreed well with the experimental observation, which indicated that our proposed model could give a good estimation of processing–crystallization kinetics–morphology relationships for PP and GFRPP.

INTRODUCTION

The investigation of crystallization kinetics of semicrystalline polymers attracted lots of attention owing to its important influence on the morphology, crystallinity, and physical and mechanical properties of products in the processing. In our previous work,[1,2] the crystallization kinetics of PP and GFRPP was analyzed for both isothermal and nonisothermal crystallization processes. Velisaris and Seferis[3] studied the crystallization mechanism and kinetics of PEEK reinforced with carbon fiber, and found smaller crystallinity and crystallization rate for this composite compared to the pure PEEK. However, Lee and Porter[4] indicated for the same composite as above that the nucleation density was higher on the surface of carbon fiber. As the content of carbon fiber increased, the degree of supercooling needed for nonisothermal crystallization would decrease, which could speed the crystallization process. When the cooling rate was lower, transcrystalline structure would be found on the surface of carbon fibers, and the overall crystallinity increased with increasing the carbon fiber. Jog and Nadkarni[5] examined the crystallization behavior of glass-fiber-reinforced PPS. They found an increase of crystallization rate, but a decrease of crystallinity with the addition of glass fiber to PPS. Campbell and Qayyum[6] put several kinds of fibers into PP and observed the growth rate of spherulites in each case. They pointed out that fibers would increase the nucleation density. Gupta et al.[7] utilized DSC to study the nonisothermal crystallization kinetics of PP/glass fiber composites. They found that fibers would induce higher crystallinity and higher crystallization rate, but the size of spherulites became smaller.

The injection molding process was generally discussed according to the three stages—filling, packing, and cooling. The temperature profiles at each stage in thin disc part of PP and GFRPP could be simulated and calculated from our program developed in the previous work.[8] Which combined with our dynamic crystallization model,[1,2] the crystallization morphologies of PP and GFRPP were predictable in the process of injection molding.

THEORETICAL TREATMENT

Dynamic Crystallization Model

The crystallization mechanism of PP was shown to be of instantaneous nucleation and spherical growth

* To whom correspondence should be addressed.

Journal of Applied Polymer Science, Vol. 43, 521–527 (1991)
 CCC 0021-8995/91/030521-07$04.00

in crystals. The growth rate of spherulites (G), the concentration of spherulites (N), and the crystallization rate constant (K) at isothermal condition were derived as[1,2]

$$N = N_0 \exp[N_1/(T_c + C_2 - T_g)] \times \exp[N_2 T_m^0/T_c \Delta T] \quad (1)$$

$$G = G_0 \exp[G_1/(T_c + C_2 - T_g)] \times \exp[G_2 T_m^0/T_c \Delta T] \quad (2)$$

$$K = K_0 \exp[K_1/(T_c + C_2 + T_g)] \times \exp[K_2 T_m^0/T_c \Delta T] \quad (3)$$

where $K = \frac{3}{4}\pi G^3 N$, T_c is the crystallization temperature, T_m^0 the limiting melting temperature, T_g the glass transition temperature, and $\Delta T = T_m^0 - T_c$.

Avrami equation was accepted in describing the relative crystallinity (X_r) of polymer at isothermal condition as follows:

$$X_r(t) = 1 - \exp(-Kt^n) \quad (4)$$

At nonisothermal condition, the concentration of spherulites was derived as[1,2]

$$N(t) = \int_0^t \dot{N}(\tau)[1 - X_r(\tau)]\, d\tau \quad (5)$$

and

$$\dot{N}(\tau) = \left.\frac{dN}{dT}\right|_{T=T(\tau)} \cdot \left.\frac{dT}{dt}\right|_{t=\tau} \quad (6)$$

The corresponding relative crystallinity was expressed as[1,2]

$$X_r(t) = X(t)/X_{l0} = 1 - \exp\left\{-\tfrac{4}{3}\pi \int_{t_0}^t \left[\int_\tau^t G(T(u))\, du\right]^3 \times N(\tau)\, d\tau\right\} \quad (7)$$

where X_{l0} is the limiting absolute crystallinity at zero cooling rate, and $X(t)$ was the absolute crystallinity at time t.

The average radius of spherulites was estimated to lie between two bounds, R_{av}^l and R_{av}^u[2]:

$$R_{av}^l = (3dX_c/4\pi N_t d_c)^{1/3} \quad (8)$$

$$R_{av}^u = (3/4\pi N_t)^{1/3} \quad (9)$$

where N_t is the concentration of spherulites, X_c the absolute crystallinity, d_c the density of crystalline phase, and d the apparent density of sample.

Once the temperature duration was given, the crystallinity, size of spherulites, and concentration of spherulites of polymer could be calculated from eqs. (1)-(9).

Injection Molding Process[8]

The mold used for simulation was a center-gated disk-shaped one, which could be visualized as 1-dimensional radial flow. The specifications of the mold were shown in Figure 1. Assuming the fluid obeyed the CEF equation, and the governing equation were as follows.[8]

At Filling Stage

Equation of continuity:

$$Q = 2\pi \int_{-b}^{b} r v_r\, dz \quad (10)$$

where Q is the volumetric flow rate and v_r the r-component velocity.

Equation of motion:

$$\frac{\partial p}{\partial r} = \frac{\partial}{\partial z}\left(\eta \frac{\partial v_r}{\partial z}\right) \quad (11)$$

where p is the pressure and η the viscosity of the fluid.

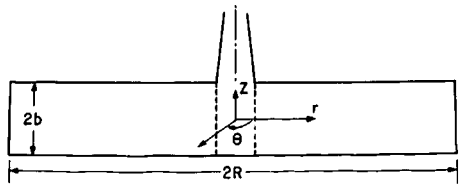

Figure 1 Schematic representation of disc mold, and the coordinate system: R = 10.16 cm, b = 0.127 cm.

Equation of energy:

$$\rho C_p\left(\frac{\partial T}{\partial t}+v_r\frac{\partial T}{\partial r}\right)=k\frac{\partial^2 T}{\partial z^2}+\eta\left(\frac{\partial v_r}{\partial z}\right)^2 \quad (12)$$

where T is the temperature, ρ the density of the fluid, C_p the heat capacity of the fluid, and k the thermal conductivity of the fluid. In above equations, the elastic effect has been proved not to be significant[8] and was neglected at filling stage for a thin disk-shape mold.

At Packing Stage

The isothermal assumption at packing stage was made, which meant that the temperature of fluid maintained at that of the end of filling stage.

Equation of continuity:

$$\frac{\partial \rho}{\partial t}+\frac{1}{r}\frac{\partial}{\partial r}(\rho r v_r)=0 \quad (13)$$

Equation of motion:

$$\frac{\partial \rho}{\partial \gamma}=\eta\frac{\partial^2 v_r}{\partial z^2} \quad (14)$$

At Cooling Stage

Assuming that the heat transfer took place only in the Z-direction, i.e.,

$$\rho C_p\frac{\partial T}{\partial t}=k\left\{\frac{\partial^2 T}{\partial z^2}+\frac{1}{k}\left[\left(\frac{\partial k}{\partial z}\right)\left(\frac{\partial T}{\partial z}\right)+\frac{T}{V}\left(\frac{\partial V}{\partial T}\right)_p\frac{dp}{dt}\right]\right\} \quad (15)$$

where V is the volume of the fluid.

From eqs. (10)–(15), the temperature variation with time at any position of disk part in injection molding process was first calculated. Then combining the dynamic crystallization model, i.e., eqs. (1)–(9), the crystallization morphology in injection molding parts of PP and GFRPP could be reasonably estimated.

EXPERIMENTAL

Materials

(1) PP, MI = 3.0 g/10 min.
(2) Glass fiber, 6 mm chopped strand, 15–22 μm in diameter, sp. gr. $\doteqdot$ 2.61.

Extrusion Blending

PP pellets or PP pellets mixed with glass fiber were well blended through an extruder. The sample containing 90 wt % PP and 10 wt % glass fiber was symbolized as 90PP/10GF. The screw speed was set at 25 rpm and the temperatures of three zones of extruder were set at 200, 210, and 220°C. The extrudate was then crushed and fed into an injection molding machine.

Injection Condition

The temperatures of three zones along screw section of injection molding machine were set at 210, 215, and 220°C, and that of die was set at 227°C. With a flow rate of 40 cm^3/s, a holding pressure of 50 bar, a holding time of 0.1 s, and a mold temperature of 311 K (or 330 K), the molten PP or GFRPP was injected into a thin disc mold with radius of 10.16 cm and thickness of 0.127 cm as shown in Figure 1.

Morphology Observation

The pictures of spherulites of PP and GFRPP in core region of molded disc part were taken through SEM. The sizes of spherulites were measured and compared with the theoretical prediction.

RESULTS AND DISCUSSION

The governing equations [(10)–(15)] of three stages in the injection molding process were solved through computer.[8] The thermal physical properties (ρ, k, C_p) and the viscosity (7) have been changed in the simulations for GFRPP versus the PP resin. Details are shown in the Appendix. With an injection rate of 40 cm^3/s, an inlet temperature of fluid at 500 K, and a mold temperature at 311 K, the variation of temperature with time in core region ($z = 0$) and in skin region ($z \to b$) of the disc part of 90PP/10GF in one injection cycle (including three stages) were simulated and are shown in Figure 2. The corresponding exothermic flux, which was proportional to the rate of change of crystallinity (dx/dt), for the crystallization of 90PP/10GF molded part was calculated from both the temperature variation with time in mold and the dynamic crystallization model [eqs. (1)–(7)]. The parameters in eqs. (1)–(7) for GFRPP and PP were summarized in tables in our previous work.[2] It was seen that the temperature dropped very rapidly in skin region and only about

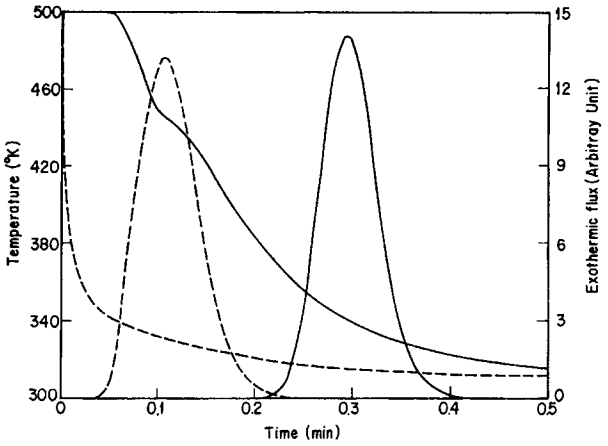

Figure 2 Simulated crystallization curves of 90PP/10GF in injection molded disc part: (——) variation of temperature with time and crystallization curve in core region; (- - -) variation of temperature and crystallization curve in skin region.

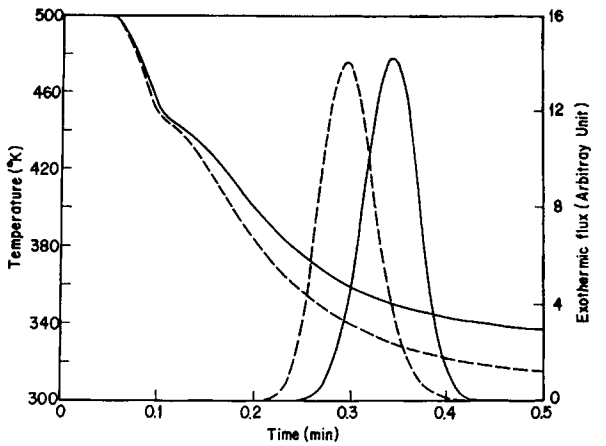

Figure 4 Crystallization curves of 90PP/10GF in core region of disc part during injection molding at different mold temperatures: (——) mold temperature at 333 K; (- - -) mold temperature at 311 K.

0.2 min was needed for complete crystallization. The maximum crystallization rate occurred at about 0.1 min, and the crystallization temperature ranged from 345 to 325 K, whereas, in the core region, the temperature dropped more slowly than that in the skin region, and about 0.4 min was needed for complete crystallization. The maximum crystallization rate occurred at about 0.3 min, and the crystallization temperature ranged from 360 to 325 K. In Figure 3, the crystallization curves and temperature variations for PP (solid lines) and 90PP/10GF (dashed lines) in the core region under the same injection molding condition were shown for comparison. The temperature of GFRPP was slightly lower than that of PP. The crystallization rate of GFRPP was higher than that of PP. Only about 0.4 min was needed for complete crystallization of GFRPP instead of 0.5 min for PP.

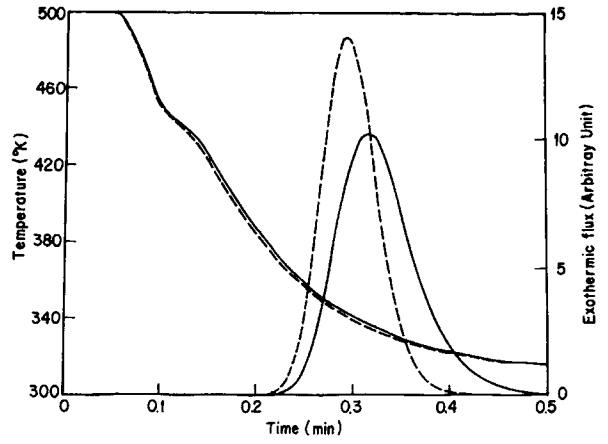

Figure 3 Comparison of crystallization curves of PP and 90PP/10GF in core region during injection molding: (——) variation of temperature and crystallization curve of PP; (- - -) variation of temperature and crystallization curve of 90PP/10GF.

Figure 4 showed in temperature variation with time and the crystallization curve of 90PP/10GF in the core region of the molded part during injection molding at different mold temperatures. When the mold temperature was higher, the crystallization would start and complete later. Figure 5 showed the SEM pictures of sperulites of PP and GFRPP in the core region of the molded disc part. It was seen from Figures 5(a) and 5(b) that GFRPP showed similar sizes of spherulites as PP at the same injection condition. When the mold temperature was higher, larger spherulites were expected and observed in Figures 5(a) and 5(c). The theoretically calculated mean radius [i.e., $(R^l_{av} + R^u_{av})/2$ from eqs. (8) and (9)] was listed for each case, which gave rather reasonable prediction on the order of magnitude of sizes.

It was concluded that the crystallization rate was very high for PP and GFRPP in injection molding process. In skin region the temperature dropped more rapidly than that in core region, and crystallization would complete in a very short time, particularly in the skin region. The average size of spherulites of GFRPP was smaller than that of PP. Our dynamic crystallization model could give reasonable prediction of crystallization morphology of PP or GFRPP in the injection molding process.

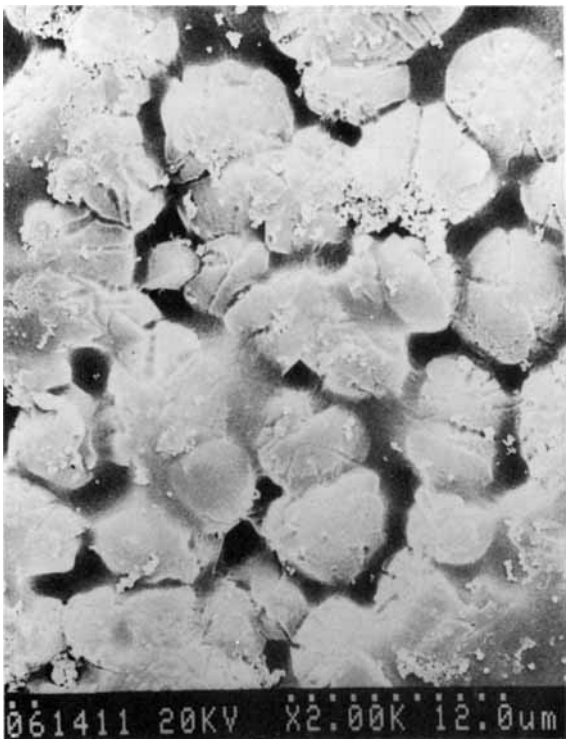

(a) PP, mold temperature = 311 K, observed mean radius: 3.0 μm.

(b) 90 PP/10 GF, mold temperature = 311 K, observed mean radius: 3.1 μm.

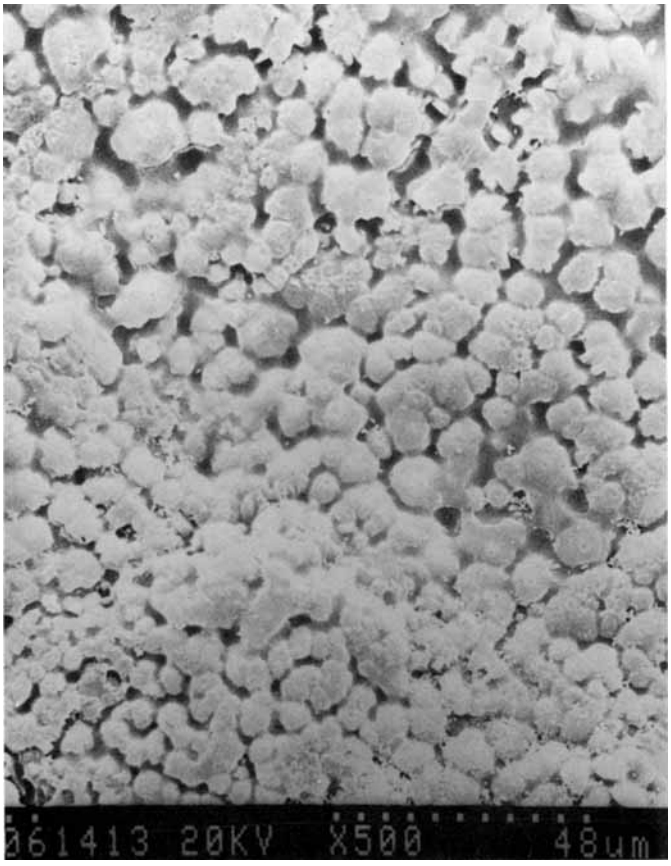

(c) PP, mold temperature = 333 K, observed mean radius = 4.9 μm.

Figure 5 Pictures of spherulites in core region of molded disc part. Theoretically calculated mean radius (μm): (a) 6.35; (b) 5.24; (c) 6.82.

APPENDIX: PHYSICAL DATA USED IN SIMULATION

Viscosity[8,9]

The mixing rule

$$\mu_c = \mu \cdot (1 + 0.5 \cdot \phi_f)/(1 - \alpha \cdot \phi_f)$$

where μ_c, μ = viscosity (g/cm s) of GFRPP and PP respectively, ϕ_f = volume fraction of glass fiber, $\alpha = 1 + \phi_f \cdot (1 - \Phi_m)/\Phi_m^2$. μ is expressed with the Cross model:

$$\mu(\dot{\gamma}, T) = \mu_0(T)/[1 + C \cdot (\mu_0(T) \cdot \dot{\gamma}]^{1-n}$$

$$\mu_0(T) = B \cdot \exp(T_b/T)$$

If $T < 440$ K,

$$\mu(\dot{\gamma}, T) = \mu_0(T)$$

Φ_m	0.82
B	9 g/cm s
T_b	4550 K
n	0.323
C	3.77E−4 (g/cm s^2)$^{n-1}$

Heat Conductivity[8,10]

$$K_c = K_P \cdot (1 + A \cdot B \cdot \phi_f)/(1 - \alpha \cdot B \cdot \phi_f)$$

where $\alpha = 1 + \phi_f \cdot (1 - \Phi_m)/\Phi_m^2$, $A = 0.5$, $\Phi_m = 0.82$, $B = (K_f/K_P - 1)/(K_f/K_P + A)$, K_c, K_f, K_P = heat conductivities (erg/cm s K) of GFRPP, glass fiber, and PP, respectively, K_f = 1.05E5 erg/cm s K. K_P is expressed as[8]

$$K_P = C_0 + C_1 \cdot T$$

and T in °C.

Range (°C)	C_0	C_1
$T \le 76$	0.1569E5	78.332
$76 \le T < 145$	0.20455E5	17.084
$145 \le T < 158$	−0.72986E5	662.45
$158 \le T < 176$	0.31495E5	0
$176 \le T < 183$	3.8504E5	−2010.6
$T > 183$	0.17433E5	0

Density and Specific Volume[8,11]

$$d_c = d_f \cdot \phi_f + d_P \cdot \phi_P$$

where ϕ_f, ϕ_P = volume fractions of glass fiber and PP, d_c, d_f, d_P = densities of GFRPP, glass fiber, and PP. In the filling stage, these are taken as constant, so that

$$d_f = 2.54 \text{ g/cm}^3, \quad d_P = 0.77 \text{ g/cm}^3$$

At the cooling stage, specific volume (in cm^3/g) GFRPP is expressed as

$$V_c = W_f \cdot V_g + W_P \cdot V_P$$

where V_c, V_f, V_P = specific volumes of GFRPP, glass fiber, and PP, respectively, W_f, W_P = weight fraction of glass fiber and PP,

$$V_g = 0.3916 + 1.8824E - 6 \cdot (T - 25), \quad T \text{ in °C}$$

and specific volume of PP is expressed by the Tait equation:

$$V(P, T) = V(0, T) \cdot \{1 - C \cdot \ln[1 + P/B(T)]\}$$

where $V(0, T) = V_0 \cdot \exp(\alpha \cdot T)$, $B(T) = B_0 \cdot \exp(B_1 \cdot T)$, P = pressure (kg/cm^2), T = temperature (°C).

α	6.7E−4°C^{-1}
B_0	1520 kg/cm^2
B_1	4.177E−3°C^{-1}
V_0	1.1606 cm^3/g
C	0.0984

Heat Capacity[12]

The mixing rule is

$$Cp_c = Cp_f \cdot W_f + Cp_P \cdot W_P$$

where Cp_c, Cp_f, Cp_P = heat capacities of GFRPP, glass fiber, and PP, respectively. (erg/g K),

$$Cp_f = 6.947E6 + 5.767E3 \cdot T, \quad T \text{ in K}$$

$$T > 450 \text{ K}, \quad Cp_P = 1.02276E7 + 3.6022E4 \cdot T$$

$$390 \text{ K} \le T < 450 \text{ K}, \quad Cp_P = -2.839E9 \cdot Q^5 + 5.669E9 \cdot Q^4 - 3.77E9 \cdot Q^3 + 1.022E9 \cdot Q^2 - 8.078E7 \cdot Q + 2.72E7$$

where $Q = (T - 390)/60$,

$$350 \text{ K} \le T < 390 \text{ K},$$

$$Cp_P = 2.3E7 + 1.588E6 \cdot Q + 2.623E6 \cdot Q^2$$

where $Q = (T - 350)/40$,

$$T \le 350 \text{ K}, \quad C_{p_P} - 2.034E6 + 7.168E4 \cdot T$$

REFERENCES

1. C. C. Fan-Chiang, Master thesis, National Taiwan University, 1987.
2. H. J. Tai, W. Y. Chiu, L. W. Chen, and L. H. Chu, *J. Appl. Polym. Sci.*, to appear.
3. C. N. Velisaris and J. C. Seferis, *Polym. Eng. Sci.*, **26,** 1574 (1986).
4. Y. Lee and R. S. Porter, *Polym. Eng. Sci.*, **26,** 633 (1986).
5. J. P. Jog and V. M. Nadkarni, *J. Appl. Polym. Sci.*, **30,** 997 (1985).
6. D. Campbell and M. M. Qayyum, *J. Polym. Sci. Polym. Phys. Ed.*, **18,** 83 (1980).
7. A. K. Gupta, V. B. Gupta, R. H. Peters, W. G. Harland, and J. P. Berry, *J. Polym. Sci. Polym. Phys. Ed.*, **27,** 4669 (1982).
8. W. Y. Chiu, L. W. Chen, C. Wang, and D. C. Wang, *J. Appl. Polym. Sci.*, to appear.
9. M. Eder and A. Wlochowicz, *Polymer,* **24,** 1593 (1985).
10. M. Sanou, B. Chung, and C. Cohen, *Polym. Sci. Eng.*, **25,** 1008 (1985).
11. K. H. Hsieh, C. C. Lee, and J. S. Tsai, *Bull. College Eng. Natl. Taiwan Univ.*, **43,** 195 (1988).
12. K. H. Hsieh and Y. Z. Wang, *Polym. Eng. Sci.*, **30**(8), 476 (1990).

Received July 30, 1990
Accepted December 4, 1990